The role of pH and dose/solubility ratio on cocrystal dissolution, drug supersaturation and precipitation

Tatiane Cogo Machado , Gislaine Kuminek ,
Simone Gonçalves Cardoso , Naír Rodríguez-Hornedo

PII: S0928-0987(20)30211-6
DOI: https://doi.org/10.1016/j.ejps.2020.105422
Reference: PHASCI 105422

To appear in: *European Journal of Pharmaceutical Sciences*

Received date: 31 March 2020
Revised date: 28 May 2020
Accepted date: 7 June 2020

Please cite this article as: Tatiane Cogo Machado , Gislaine Kuminek , Simone Gonçalves Cardoso , Naír Rodríguez-Hornedo , The role of pH and dose/solubility ratio on cocrystal dissolution, drug supersaturation and precipitation, *European Journal of Pharmaceutical Sciences* (2020), doi: https://doi.org/10.1016/j.ejps.2020.105422

Highlights

- Cocrystal dissolution interfacial pH mitigates drug dissolution-pH dependence
- Cocrystal to drug conversion occurs via surface nucleation of metastable polymorph
- σ_{max} and AUC decrease with decreasing Do as dissolution media pH increase
- When Do>>SA, drug supersaturation is sustained for very long times
- When Do<<SA, σ_{max} approaches Do, C_{max} approaches the full dose concentration C_{dose}

The role of pH and dose/solubility ratio on cocrystal dissolution, drug supersaturation and precipitation

Tatiane Cogo Machado[a], Gislaine Kuminek[b], Simone Gonçalves Cardoso[a], Naír Rodríguez-Hornedo[b,*]

[a]Programa de Pós-Graduação em Farmácia, Universidade Federal de Santa Catarina, Florianópolis 88040-900, SC, Brazil.

[b]Department of Pharmaceutical Sciences, College of Pharmacy, University of Michigan, Ann Arbor, Michigan 48109-1065, United States.

[*] Corresponding author.
Telephone: +1-7347630101; Fax: +1-7346156162. College of Pharmacy, 428 Church Street, University of Michigan, Ann Arbor, MI 48109-1065; E-mail address: nrh@umich.edu

ABSTRACT

Cocrystals that are more soluble than the constituent drug, generate supersaturation levels during dissolution and are predisposed to conversion to the less soluble drug. Drug release studies during cocrystal dissolution generally compare several cocrystals and their

crystal structures. However, the influence of drug dose and solubility in different dissolution media has been scarcely reported. The present study aims to investigate how drug dose/solubility ratio ($Do=C_{dose}/S_{drug}$), cocrystal solubility advantage over drug ($SA=S_{cocrystal}/S_{drug}$), and dissolution media affect cocrystal dissolution-drug supersaturation and precipitation (DSP) behavior. SA and K_{sp} values of 1:1 cocrystals of meloxicam-salicylic acid (MLX-SLC) and meloxicam-maleic acid (MLX-MLE) were determined at cocrystal/drug eutectic points. Results demonstrate that both cocrystals enhance SA by orders of magnitude (20 to 100 times for the SLC and over 300 times for the MLE cocrystal) in the pH range of 1.6 to 6.5. It is shown that during dissolution, cocrystals regulate the interfacial pH (pH_{int}) to 1.6 for MLX-MLE and 4.5 for MLX-SLC, therefore diminishing the cocrystal dissolution rate dependence on bulk pH. Do values ranged from 2 (pH 6.5) to 410 (pH 1.6) and were mostly determined by the drug solubility dependence on pH. Drug release profiles show that maximum supersaturation ($\sigma_{max}=C_{max}/S_{drug}$) and AUC increased with increasing Do as pH decreased. When Do>>SA, the cocrystal solubility is not sufficient to dissolve the dose so that a dissolution-precipitation quasi-equilibrium state is able to sustain supersaturation for the extent of the experiment (24 hours). When Do<<SA, cocrystal solubility is more than adequate to dissolve the dose. Low σ_{max} values (1.7 and 1.5) near the value of Do (2.3 and 2.4) were observed, where a large fraction of the cocrystal added is dissolved to reach σ_{max}. Two different cocrystal to drug conversion pathways were observed: (1) surface nucleation of the metastable MLX polymorph IV on the dissolving cocrystal preceeded formation of the stable MLX polymorph I in bulk solution (in all conditions without FeSSIF), and (2) bulk nucleation of the stable MLX polymorph (in FeSSIF). The interplay between cocrystal SA, Do, and drug precipitation pathways provide a framework to interpret and understand the DSP behavior of cocrystals.

Keywords

cocrystal; dose number; disproportionation; precipitation; supersaturation, interfacial pH

1. Introduction

Drug solid-state forms such as salts, cocrystals and amorphous solids have been shown to increase drug exposure by enhancing solubility and generating supersaturated drug

solutions, especially for Biopharmaceutics Classification System (BCS) class II drugs, which have high permeability and low solubility (Amidon et al., 1995; Berry and Steed, 2017; Bevernage et al., 2013; Lakshman et al., 2020; Sun and Lee, 2015; Tanaka et al., 2017; Taylor and Zhang, 2016). The bioavailability advantage of these solid-state forms is dependent on sustaining supersaturation levels during dissolution, achieved by different approaches depending on the chemistry and structure of the solid-state and their associated solution chemistry (Alhalaweh et al., 2014; Bevernage et al., 2013; Greco and Bogner, 2011; Leyssens and Horst, 2018; Sun and Lee, 2015). Pharmaceutical cocrystals that solve bioavailability problems due to the drug insufficient solubility to dissolve the dose are supersaturating systems. These cocrystals are also referred to as incongruent systems and they are the subject of this manuscript.

Cocrystals are a single phase with well-defined stoichiometry, composed of two or more different molecular components that are solid at room temperature. Cocrystals can enhance the solubility-pH dependence of a drug, furthermore cocrystals can modulate the dissolution dependence on pH, by altering the microenvironment pH (Cao et al., 2019, 2016; Chen and Rodríguez-Hornedo, 2018; Huang et al., 2019). Cocrystal stoichiometry, ionization, and hydrophilicity of its components provide unique control over cocrystal solubility and supersaturation with respect to drug. Furthermore, cocrystal solubility is dependent on solution conditions and a cocrystal that is more soluble than the drug can become less soluble, by changing solution pH or by reducing the drug thermodynamic activity such as by drug solubilization in micelles or complexes in solution (Lipert and Rodríguez-Hornedo, 2015).

Meloxicam (MLX), a nonsteroidal anti-inflammatory drug (NSAID) is a BCS Class II drug (Amidon et al., 1995; Del Tacca et al., 2002; Türck et al., 1995). MLX is zwitterionic with pK_a values of 1.09 (acidic group) and 4.18 (basic group) (Luger et al., 1996; Machado et al., 2018). As a consequence of its poor solubility in acidic aqueous conditions, MLX is slowly absorbed, with peak plasma concentrations attained after approximately 10 hours (Davies and Anderson, 1997). Solubility measurements from the present work show that the highest marketed dose of MLX (15 mg) exceeds drug solubility by a factor of 120 to 21 at pH range values of 1.0 to 5.0, which means that less than 5.0 % of this dose will dissolve in 250 mL (luminal volume) over the same pH range. Whereas, under intestinal pH (>6.5) the entire drug dose will dissolve. In view of this, numerous strategies have been considered to improve MLX solubility, enhance its dissolution rate, and accelerate its therapeutic onset. Approaches such as self-nanoemulsifying, micellar solubilization, nanosuspension, salt formation, cyclodextrin inclusion complexes, nanocrystals and cocrystals have been published (Badran et al., 2014; Cheney et al., 2010; Ghorab et al., 2004; Ochi et al., 2013, 2014; Ullah and Kaleem, 2011; Weyna et al., 2012).

While most cocrystal dissolution studies in the literature have focused on the shape of drug concentration-time profiles, in this present work we consider the cocrystal solubility advantage ($SA=S_{cocrystal}/S_{drug}$) and dose/solubility ratio ($Do=C_{dose}/S_{drug}$), in analyzing cocrystal dissolution and drug supersaturation-precipitation (DSP) profiles. SA is proportional to the free energy for drug nucleation and its value represents the cocrystal potential for conversion to the less soluble drug. Do is the answer to the question: Will the drug solubility be enough for the dose to dissolve? If Do is less than 1, the full dose

will dissolve. If it is above 1, the drug solubility is not enough to dissolve the dose. This concept was initially introduced by Oh et al. (1993) to quantify the volume of fluid necessary to dissolve the entire drug dose and has been of great utility to classify oral absorption limitations (Oh et al., 1993). The total dose is divided by the volume of fluid (e.g., gastric, intestinal or other fluid of interest) to obtain the dissolved dose concentration (C_{dose}), and when compared to the drug solubility (S_{drug}) under the same conditions provides the extent to which the full dose will dissolve (Sugano and Terada, 2015). This assumes a closed system (no absorption).

The role of dose/solubility ratio on dissolution of non-supersaturating systems and bioavailability from the GI tract has been established (Rinaki et al., 2004). The importance of dose on drug release profiles and supersaturation of amorphous solid dispersions has been recently demonstrated (Schver and Lee, 2018). To our knowledge, these concepts have not been considered for cocrystals.

We propose that Do is also a measure of the solubility enhancement necessary to dissolve the dose via high-energy solid forms such as cocrystals. In this context the value of Do represents the supersaturation needed to dissolve the dose. While the required supersaturations may not be achievable or kinetically sustained, they allow for classifying cocrystals in terms of Do and SA to explain DSP profiles.

Do varies with dose and drug solubility. SA can be modulated by cocrystal components solubilities, ionization, and by the presence of drug solubilizing agents such as physiologically relevant surfactants composed of bile salts and phospholipids (Good and Rodríguez-Hornedo, 2009; Kuminek et al., 2016; Chen and Rodríguez-Hornedo, 2018). The present study provides a framework to understand how Do and SA,

influences DSP profiles as a function of pH and in the presence of the biorelevant medium fed state simulated intestinal fluid (FeSSIF) compared to the pure drug. MLX cocrystals with monoprotic and diprotic coformers were investigated. This study aims to (1) evaluate the drug and cocrystal solubility ($S_{cocrystal}$) dependence on pH and the influence of FeSSIF (2) determine the thermodynamic parameters: solubility product (K_{sp}), eutectic constant (K_{eu}) and solubility advantage (SA) that describe cocrystal solubility, and (3) determine how SA and Do influence drug release, supersaturation levels, and precipitation pathways during cocrystal dissolution.

2. Materials and methods

2.1 Materials

2.1.1 Cocrystals components. Meloxicam form I (MLX) was purchased from Technodrugs & Intermediates (Gujarat, India). Maleic acid (MLE) was purchased from Merck (Darmstadt, Germany), and salicylic acid (SLC) was purchased from Xiamen Fine Chemical (Xiamenn, China). Drug and coformers were characterized by X-ray powder diffraction (XRPD) and differential scanning calorimetry (DSC) before experiments were carried out.

2.1.2 Solvents and buffer components. Ethyl acetate and tetrahydrofuran (analytical grade), methanol and acetonitrile (High performance liquid chromatography (HPLC) grade) were purchased from Tedia (Rio de Janeiro, Brazil). Sodium hydroxide, acetic acid, sodium acetate, and sodium chloride were purchased from Sigma (St. Louis, MO). FaSSIF/FeSSIF/FaSSGF powder (Version 1) was acquired from Biorelevant.com LTD (London, UK). Water used in these studies was filtered through a purification system (Milli-Q® Water System) from Millipore Co. (Bedford, MA).

2.2 Methods

2.2.1 Cocrystal Synthesis. Cocrystals were prepared by reaction crystallization method at room temperature (Rodríguez-Hornedo et al., 2006). The 1:1 meloxicam-salicylic acid cocrystal (MLX-SLC) was prepared by adding MLX to nearly saturated solution of SLC in ethyl acetate, and 1:1 meloxicam-maleic acid cocrystal (MLX-MLE) was prepared by adding MLX to nearly saturated MLE solution in tetrahydrofuran. The suspensions were stirred for 24 hours. Solid phases were characterized by XRPD and DSC (see supplementary material Figure S1 – S4) and stoichiometry (purity) was verified by HPLC. Full conversion to cocrystal was observed in 24h.

2.2.2 Solubility and dissolution media preparation. HCl solutions (0.1 M and 0.001 M) at pH values of 1.0 and 3.0, respectively, were prepared by diluting concentrated hydrochloric acid solution (12 M). pH 1.6 (±0.02) buffer (34 mM) was prepared with the appropriate amount of NaCl and HCl solutions. pH 5.0 (±0.01) acetate buffer (144 mM) (blank FeSSIF) was prepared with the appropriate amount of NaOH (pellets), acetic acid, and NaCl in water. FeSSIF was prepared by dissolving the appropriate amount of FaSSIF/FeSSIF/FaSSGF powder in blank buffer pH 5.0, according to manufacturer protocols (Biorelevant.com LTD). pH 6.52 (±0.02) phosphate buffer was prepared with appropriate amount of sodium chloride (105.9 mM), monobasic sodium phosphate (28.4 mM) and sodium hydroxide (8.7 mM) in water. The pH values of all media were adjusted to target pH with 1 M NaOH and 1 M HCl solutions. Water was filtered through a double deionized purification system (MilliQ®) and the pH measured was 6.3.

2.2.3 Drug solubility. Drug solubility was measured by adding excess solid to 30 ml of solution media. The suspensions were magnetically stirred and maintained at 25 ± 0.2°C

using a water bath until equilibrium was reached (48-72 h). At 24 h intervals, pH was measured, and 5 mL aliquots were taken and filtered through a 0.45 µm pore membrane. The solution concentrations of MLX were analyzed by HPLC. Solid phases in equilibrium were characterized by XRPD and DSC.

2.2.4 Cocrystal Solubility Measurements. The cocrystal equilibrium solubility was determined at the eutectic point, where drug and cocrystal solid phases are in equilibrium with the solution. An excess amount of each solid phase was added to 30 mL of solution media, and the suspensions were magnetically stirred and maintained at 25 ± 0.2°C using a water bath until equilibrium was reached (48-72 h). At 24 h intervals, pH was measured, and 2 mL aliquots were taken and filtered through a 0.45 µm pore membrane. The solid phases were also collected at 24 h intervals and characterized by XRPD and DSC to ensure the sample was at the eutectic point (confirmed by presence of both drug and cocrystal solid phases and constant drug and coformer solution concentrations). The filtered solutions were analyzed by HPLC in order to obtain the drug and coformer concentrations.

Cocrystal stoichiometric solubilities were calculated from measured total eutectic concentration of drug and coformer ($[drug]_{T,eu}$ and $[coformer]_{T,eu}$) according to the following equation for 1:1 cocrystals:

$$S_{cocrystal}^{1:1} = \sqrt{[drug]_{T,eu}[coformer]_{T,eu}} \quad (1)$$

where $S_{cocrystal}$ is the total cocrystal solubility, the terms in brackets represent molar concentrations under equilibrium conditions and subscript T represents total concentration of all species.

Cocrystals dissociate in solution into drug and coformer, and the equilibrium between the solid cocrystal and the molecular constituents in solution is expressed by a constant, which is known as the solubility product (K_{sp})

$$\left(\text{drug}_\text{y}\text{coformer}_\text{z}\right)_{\text{cocrystal}} \overset{K_{sp}}{\longleftrightarrow} \text{ydrug}_{\text{soln}} + \text{zcoformer}_{\text{soln}} \quad (2)$$

where y and z represent the stoichiometric coefficients of the drug and coformer, respectively.

MLX-SLC and MLX-MLE cocrystal solubility product (K_{sp}) was determined from eutectic concentrations of drug and coformer measured according to

$$K_{sp} = [^{+}\text{MLX}^{-}]_0\,[\text{HA}]_0 \quad (3)$$

for MLX-SLC, and

$$K_{sp} = [^{+}\text{MLX}^{-}]_0\,[\text{H}_2\text{A}]_0 \quad (4)$$

for MLX-MLE.

$[\text{drug}]_0$ and $[\text{coformer}]_0$ represent the molar concentration of the neutral species of drug and coformer at eutectic point. The zwitterionic form of MLX in the cocrystal is here referred to as the neutral species of MLX.

2.2.5 Dissolution studies. Cocrystals and drug powder dissolution studies were conducted in triplicate in buffer pH 1.6, blank FeSSIF pH 5.0 and FeSSIF pH 5.0. The temperature was maintained at 25.0 (± 0.2) °C and the stirring rate was 150 rpm using a shaker incubator (NT715 Nova Técnica, Brazil) for up to 24 h. 10 mg of MLX drug or MLX-equivalent amount of cocrystal were added in 50 mL of dissolution media. Both drug and cocrystal powders were sieved through a mesh (125 µm) before carrying out experiments. Solution pH was measured at the beginning and at the end of each dissolution experiment. Aliquots of 1.0 mL were taken with a syringe at time points up

to 24 h and filtered through a 0.45 µm pore membrane. Concentrations of drug and coformer were analyzed by HPLC. The final solid phases were characterized by DSC and Fourier transform infrared (FT-IR) spectroscopy.

2.2.6 Dose solubility ratio. Human Do was calculated according to

$$\mathrm{Do} = \frac{C_{dose}}{S_{drug,T}} = \frac{M_0/V_0}{S_{drug,T}} \quad (5)$$

where C_{dose} is defined by the drug marketed dose (mmol) (M_0) divided by the volume (L) taken with dose or luminal volume (0.25 L) (V_0), and $S_{drug,T}$ is the drug solubility (mM). Doses are generally reported in the literature in mg. Here we convert the drug dose to a molar scale (millimoles) and concentrations are in millimoles/L (mM).

In vitro Do was calculated considering the C_{dose} in the dissolution experiments, which was obtained from the MLX-equivalent amount of cocrystal added in the media (see dissolution methods 2.2.5).

2.2.7 High-performance Liquid Cromatography (HPLC). Solution concentrations of drug and coformer were analyzed by Shimadzu LC-10 HPLC (Columbia, MD) equipped with an ultraviolet-visible spectrometer detector set at 360 nm for MLX, 230 nm for SLC and 240 nm for MLE. A reverse phase Phenomenex® Gemini C18 column (5 µm, 250 mm x 4.6 mm) maintained at 25 ± 0.1°C was employed. For MLX-SLC the mobile phase consisted of acetonitrile and 25 mM ammonium acetate buffer pH 6.8 and the elution was gradient from 20:80 to 80:20 proportion (acetonitrile:buffer:). For MLX-MLE the mobile phase consisted of acetonitrile, methanol and 25 mM ammonium acetate buffer adjusted to pH 2.5. The elution was gradient from 2:98 (methanol:buffer) to 90:10 proportion (acetonitrile: buffer). The sample injection volume was 20 μL and a flow rate of 1 mL/min was used for all samples.

2.2.8 X-ray Powder Diffraction (XRPD). Diffractograms were obtained using a *θ–θ* X-ray diffractometer Bruker D2 Phaser (Billerica, MA) operating with copper Kα radiation (λ = 1.5418 Å), at a current of 10 mA and voltage of 30 kV. Detection was performed on a scintillation counter one-dimensional LYNXEYE detector. The measurements were performed at room temperature, scanning at 2θ from 5° to 35°, with a 0.091° step size. Results were compared to diffraction patterns reported in literature or calculated from crystal structures reported in the Cambridge Structural Database (CSD).(Cheney et al., 2010)

2.2.9 Differential Scanning Calorimetry (DSC). DSC analyses were carried out in a Shimadzu DSC-60 cell Instrument (Columbia, MD) operating in a temperature range of 25-280°C. Samples weighing approximately 1.5 mg were heated at a rate of 10°C/min under nitrogen gas atmosphere (100 mL/min). Standard aluminum pans were used for all measurements. The DSC cell was calibrated with indium (T_{peak} 156°C; $\Delta H_{fusion\ peak}$ = 28.54Jg^{-1}) and zinc (T_{peak} 419°C). The obtained data were processed in TA-60 software.

2.2.10 Fourier transform infrared (FT-IR) spectroscopy. FT-IR spectra were obtained on a Frontier Spectrometer (PerkinElmer, Waltham, U.S.) in a frequency range from 600 to 4000 cm^{-1} at room temperature. A total of 20 scans were collected for each sample at a resolution of 4 cm^{-1}.

2.2.11 Optical microscopy. Cocrystal dissolution and drug precipitation in buffer pH 1.6, blank FeSSIF pH 5.0, FeSSIF pH 5.0 and buffer pH 6.5 were studied in suspension under bright field microscopy using a Leica Dmi8 inverted optical microscope (Wetzlar, Germany). Aliquots of 200 µL were taken during cocrystal dissolution (same condition as those in dissolution studies described above) and transferred to 96-well plates. Images

were collected with a Leica DMC2900 camera controlled with LAS v4.7 software (Leica Microsystems, Wetzlar, Germany).

2.2.12 Raman spectroscopy. Raman spectra were recorded using a Renishaw InVia Raman Microscope spectrometer equipped with wavelengths of 532, 633, and 785 nm (Renishaw Plc., UK). Spectra were recorded over the region 1200-200cm^{-1} with a resolution of 1cm^{-1}. Data analysis was performed using Spekwin®32 software.

2.2.13 Wettability studies. The OCA 15EC Contact Angle System (Filderstadt, Germany) was used for studies of the wettability of MLX, MLX-SLC, and MLX-MLE. Compacts were prepared by compressing powder (200 mg) under a pressure of 1 tonnes using a Specac hydraulic press (Specac Limited, England). The contact angles were determined after one drop of each media (buffer pH 1.6, blank FeSSIF pH 5.0, FeSSIF pH 5.0 and buffer pH 6.5) had been placed on the surface of the compacts. The change in the contact angle was measured from 1 to 10 seconds, using a goniometer. All measurements were performed in triplicate under ambient conditions of 25 (± 5) °C.

3. Results and discussion

3.1 Cocrystal K_{eu}, SA, and solubility

K_{eu} was evaluated as a function of pH in buffers and in FeSSIF (pH 5.0) by measuring the drug and coformer solution concentrations in equilibrium with cocrystal and drug solid phases at eutectic points (supplementary material Figure S5). The eutectic points in this work are between cocrystal and solid drug, since $S_{coformer} >> S_{drug.}$ When cocrystals transform to drug it is the cocrystal/drug eutectic point that is relevant. It is also important to mention that there are cocrystals where the coformer is less soluble than

drug, which utilize the eutectic associated with solid cocrystal and coformer to assess cocrystal solubility (Rosa et al., 2019).

The cocrystal solubility advantage over drug (SA) was determined from the eutectic constant K_{eu}, according to the following relationship for 1:1 cocrystals:

$$K_{eu}^{1:1} = \frac{[\text{coformer}]_{eu}}{[\text{drug}]_{eu}} = \left(\frac{S_{cocrystal}}{S_{drug}}\right)^2 = (SA)^2 \quad (6)$$

where the terms in brackets refer to molar concentrations. The Eq. (6) that relates K_{eu} and SA is obtained by expressing $S_{cocrystal}$ in Eq. (1) in terms of S_{drug} and K_{eu} by considering that $S_{drug} = [drug]_{eu}$ under the studied experimental conditions. This relationship and its application to assess cocrystal thermodynamic stability has been demonstrated for numerous cocrystals (Alhalaweh et al., 2014; Good and Rodríguez-Hornedo, 2009). SA is a measure of the potential for cocrystal to drug conversion. As SA increases, the thermodynamically achievable supersaturation with respect to drug increases up to a kinetic supersaturation threshold where drug nucleation occurs (Huang et al., 2019).

Figure 1 shows the influence of pH and biorelevant media (FeSSIF) on K_{eu} and SA values for MLX-SLC and MLX-MLE cocrystals. All K_{eu} values are > 1, indicating that both cocrystals are more soluble than MLX in this pH range. The higher the K_{eu}, the higher is SA. In fact, K_{eu} values are above 100, and since SA is the square root of K_{eu}, then SA is greater than 10 for these cocrystals in all conditions studied. MLX-MLE is shown to be the more soluble cocrystal, exhibiting the highest K_{eu} and SA values. Both parameters are also shown to increase with pH as a result of coformer ionization. The acidic coformers used in this work exhibit increased ionization at pH values above its p*K*a (3.0 for SLC and 1.9 for MLE). As a consequence, cocrystal solubility and its thermodynamic parameters (*K*eu and SA) will increase with pH. Experimental SA

values ranged from 18 to 87 for MLX-SLC in the pH range of 1.09 to 4.7, and from 304 to 371 for MLX-MLE in the pH range of 1.01 to 1.85. Although initial pH values were between 1 and 6.5, the eutectic or equilibrium pH for the MLE cocrystal equilibrated to 1.85 due to coformer self-buffering.

Figure 1

FeSSIF reduced SA values for both cocrystals (87 to 34 for MLX-SLC) and (314 to 167 for MLX-MLE). Lecithin and sodium taurocholate in FeSSIF are known to form mixed micelles in solution that preferentially solubilize the hydrophobic drug over the hydrophilic coformer, leading to a reduction of K_{eu} and SA (Lipert and Rodríguez-Hornedo, 2015).

Drug and cocrystal solubilities in Figure 2 increase with increase in pH, as expected from K_{eu} and SA results. While drug and cocrystal solubilities increase in FeSSIF, compared to buffer (blank FeSSIF), cocrystal solubilization is lower than that of the drug. The reason for this behavior is the preferential solubilization of drug in FeSSIF and follows the well recognized relationship between drug and cocrystal solubilization ratios: $SP_{cocrystal} = \sqrt{SP_{drug}}$, where SP represents the solubilization power (Lipert et al., 2015). SP is obtained from the ratio of solubility in FeSSIF and in blank FeSSIF ($SP = S_{FeSSIF}/S_{blank\ FeSSIF}$). SP values are higher for drug than for cocrystals (5.7 for MLX vs 2.4 for MLX-SLC at pH 4.70, and 5.0 for MLX vs 2.2 for MLX-MLE at pH1.84).

Figure 2

3.2 Cocrystals modulate the microenvironment pH

Figure 3 shows the initial and equilibrium pH values at saturation from solubility experiments with drug and cocrystals. Initial pH represents the bulk pH (pH_{bulk}) whereas the equilibrium pH at saturation is well recognized to be an indicator of the interfacial or microenvironment pH (pH_{int}) for ionizable compounds and their salts (Mooney et al., 1981; Serajuddin, 2007). In the case of cocrystals, pH_{int} is obtained at the equilibrium pH at the eutectic where the solution is doubly saturated with respect to cocrystal and drug.

In contrast to the drug where $pH_{int} = pH_{bulk}$, cocrystals exhibited $pH_{int} < pH_{bulk}$. As demonstrated by the results in Figure 3, cocrystals reached a constant pH value above a specific pH_{bulk} corresponding to pH_{int}. The value of pH_{int} is cocrystal dependent. This is due to acidic coformers that lower the pH at the dissolving cocrystal interface (Cao et al., 2019). pH_{int} was lower for the cocrystal with the stronger acid MLE (1.6) than for SLC (4.5). The ability of cocrystals to modulate the microenvironment pH at the dissolving surface can alter cocrystal dissolution and the drug supersaturation they generate since cocrystal SA changes with pH. SA for MLX cocrystals are expected to be lower at the dissolving surface than in the bulk solution since SA decreases with pH as already shown in Figure 1.

Figure 3

Cocrystal and drug dissolution at 30 minutes (Table 1) show that both drug and SLC cocrystal exhibit pH dependent dissolution, whereas MLE cocrystal does not. This behavior is explained by the pH_{int} of cocrystals, 4.5 for SLC and 1.6 for MLE as described above and shown in Figure 3.

Table 1. Percent cocrystal dissolved as function of bulk pH and MLX solid phase.

% dose dissolved at 30 mins			
pH_{bulk}	MLX	MLX-SLC[a]	MLX-MLE[a]
1.6	0.1	9.0	46.0
5.0	0.6	26.2	47.6
6.5[b]	3.7	54.8	46.2

[a] Percent cocrystal dissolved is independent of drug precipitation. It is determined from the mass of coformer dissolved relative to the initial coformer (cocrystal mass) according to % cocrystal dissolved $= \frac{\text{moles of coformer dissolved}}{\text{initial moles of cocrystal added}} 100$.

[b] From Weyna et al. (Weyna et al., 2012).

3.3 Drug and cocrystal solubility dependence on pH

Cocrystal solubility as a function of pH (Fig.4) was predicted from previously reported solubility equations for cocrystals composed of zwitterionic drug and acidic coformer by considering the chemical and phase equilibria and their equilibrium constants (Bethune et al., 2009).

For the drug MLX, the solubility as a function of pH is given by:

$$S_{drug} = S_{drug,0}\left(1 + 10^{(pK_{a1} - pH)} + 10^{(pH - pK_{a2})}\right) \quad (7)$$

where $S_{drug,0}$ represents the intrinsic MLX solubility (zwiterionic conditions) and pK_a is – log (ionization constant, K_a). MLX intrinsic solubility was determined to be 9.3 (±0.2) x 10^{-4} mM by fitting Eq. (7) to measured drug solubility values as a function of pH.

For MLX-SLC, where SLC is a monoprotic acid, the cocrystal solubility as a function of pH is given by:

$$S^{1:1}_{cocrystal} = \sqrt{K_{sp}\left(1 + 10^{(pK_{a1,drug} - pH)} + 10^{(pH - pK_{a2,drug})}\right)\left(1 + 10^{(pH - pK_{a1,coformer})}\right)} \quad (8)$$

For MLX-MLE, where MLE is a diprotic acid, the cocrystal solubility as a function of pH is given by:

$$S_{\text{cocrystal}}^{1:1} = \sqrt{K_{\text{sp}}\left(1 + 10^{(\text{p}K_{\text{a1,drug}} - \text{pH})} + 10^{(\text{pH} - \text{p}K_{\text{a2,drug}})}\right)} \times \sqrt{\left(1 + 10^{(\text{pH} - \text{p}K_{\text{a1,coformer}})} + 10^{(2\text{pH} - \text{p}K_{\text{a1,coformer}} - \text{p}K_{\text{a2,coformer}})}\right)} \quad (9)$$

where K_{sp} is the cocrystal solubility product. Values for equilibrium constants are presented in Tables 2 and 3.

Table 2. Cocrystal component pK_a values.

Cocrystal Component	pK_{a1}, pK_{a2}
MLX (zwiterionic)	1.09 and 4.18[a]
SLC (monoprotic acid)	3.0[b]
MLE (diprotic acid)	1.9 and 6.6[c]

[a] Reference (Luger et al., 1996)
[b] Reference (Smith, 2001)
[c] Reference (Dawson et al., 1960)

Table 3. K_{sp}, pK_{sp}, intrinsic solubility and solubility advantage of MLX cocrystals. Higher K_{sp} implies higher cocrystal intrinsic solubility.

Cocrystal	K_{sp} (M^2)	pK_{sp}[a]	S_0 (mM)[b]	SA=($S_{cocrystal}/S_{drug}$)[c] pH 1.0 to 7.0
MLX-SLC	9.81 (±1.15) x 10^{-10}	9.01	0.03 ±0.002	18 to 145
MLX-MLE	2.03 (±0.20) x 10^{-7}	6.69	0.45 ±0.023	305 to 15190

[a] pK_{sp} = - log (K_{sp}).
[b] Cocrystal intrinsic solubility obtained from $S_0 = \sqrt{K_{sp}}$
[c] Solubility advantage obtained from $S_{cocrystal}$ and S_{drug} values obtained from Eqs. (7), (8) and (9).

Cocrystal K_{sp} values in Table 3 were obtained from Eqs. (3) and (4) by considering the concentration product of neutral species of drug and coformer at equilibrium at the eutectic point. pK_{sp} values are 9.01 for MLX-SLC and 6.69 for MLX-MLE. The higher the pK_{sp} value the lower the K_{sp} and the lower the intrinsic solubility. These pK_{sp} values are in the lower half of reported (1:1) cocrystal solubilities for BCS class II drugs, which have pK_{sp} values in the range of 1 to 10 (Cavanagh et al., 2018).

Figure 4 shows that besides increasing solubility, cocrystals modulate solubility

dependence on pH. Cocrystal solubilities increase at pH ≥ coformer pK_a. While the solubilities were not able to be measured at higher pH values due to self-buffering of cocrystal components, they are a useful indicator of solubility advantage increases at high pH values that may occur during transient and non-equilibrium conditions.

MLX solubility vs pH exhibits a wide "U shape" curve. The lowest solubility occurs between pH 2 and 4 (a plateu region) and solubility increases by 2 fold at pH 1, which is related to its ionization constant (pK_{a1} 1.09), and increases exponentially at pH values above its pK_{a2} value (pK_{a2} 4.18). These results demonstrate that pH has a huge influence on drug and cocrystal solubilities. Solubility values in FeSSIF are shown in the plot and are above the curves due to the cocrystal and drug solubilization by the additive.

Figure 4

Cocrystal solubility appears to correspond with coformer solubility. MLE solubility is 450 - 17500 times higher than SLC solubility in the pH range from 1 to 7, which led to higher K_{eu} and SA values for MLX-MLE than for MLX-SLC. Furthermore, K_{sp} for MLX-MLE is 250 times higher than that of MLX-SLC, a trend consistent with coformer solubility. When solubility is determined by solvation and not by lattice energy, cocrystal solubility is dependent on the solubility of its components. Coformers appear to decrease the solvation barrier for cocrystals of hydrophobic drugs to an extent proportional to that of the pure coformer (Good and Rodríguez-Hornedo, 2009; Kuminek et al., 2016).

3.4 Importance of drug dose/solubility ratio

The problem with just considering drug release-time profiles is that dose and solubility in different media are not taken into account. These parameters are critical in determining kinetic processes of cocrystal dissolution, drug supersaturation and precipitation. Table 4 shows the drug dose/solubility ratios (Do) for MLX that correspond to human dose and dissolution doses studied in vitro in this and other work (Weyna et al., 2012). For a constant dose, Do decreases as solubility increases with pH. All Do values in Table 4 are above 1, since the drug solubility cannot meet the dose demand in all conditions studied except at pH 6.5 in humans.

Table 4. MLX dose, C_{dose} and dose/solubility ratio in different dissolution conditions.

	Drug Dose (mg)	C_{dose} (mM)	pH	S_{drug} (mM)	Do (C_{dose}/S_{drug})
Human	15	0.17[a]	1.6	1.40×10^{-3}	120
			5.0	8.00×10^{-3}	21
			6.5	3.20×10^{-1}	0.5
This study	10	0.57[b]	1.6	1.40×10^{-3}	410
			5.0	8.00×10^{-3}	70
			5.0 + FeSSIF	4.10×10^{-2}	14
Weyna et al. study	36[c]-38[d]	1.02[c] - 1.07[d]	6.5	4.38×10^{-1}	2.3 -2.4

[a]Obtained from the highest marketed solid dose of MLX (15 mg) in 250 mL.
[b]Obtained from the dissolution in vitro dose of MLX (10 mg) in 50 mL of dissolution media.
[c]Obtained from the dissolution in vitro dose of 50 mg MLX-SLC in 100 mL of dissolution media (Weyna et al., 2012).
[d]Obtained from the dissolution in vitro dose of 50 mg MLX-MLE in 100 mL of dissolution media (Weyna et al., 2012)

The dose and consequently Do values used in our dissolution studies are different from those reported by Weyna et al. and both are higher than human dose. Higher doses are generally useful to study dissolution and conversions of metastable solids as the bulk supersaturation and conversion pathways are more readily measurable. Similar approaches have also been utilized in studying amorphous solid dispersions (Schver and

Lee, 2018; Sun and Lee, 2015). Do will be further discussed in the next section to assess drug release profiles, drug supersaturation, and precipitation behavior.

3.5 Drug concentration and supersaturation vs time profiles during cocrystal dissolution

Figure 5 shows that cocrystals achieved higher drug concentrations by at least 3 times higher than drug dissolution in all media. The increase of drug release with pH is highest at the lower pH values and is superior for the less soluble cocrystal, MLX-SLC. This behavior is demonstrated by enhancement in the relative area under the curve ($RAUC=AUC_{cocrystal}/AUC_{drug}$) presented in a subsequent figure (Fig. 7) and in supplementary material Table S1. Cocrystals increase RAUC by 3 to 12 times (SLC) and 2 to 10 times (MLE).

Figure 5

Figure 6 shows that the maximum supersaturation ($\sigma_{max}=C_{max}/S_{drug}$) decreases with increasing pH as Do decreases. Both cocrystals generate σ_{max} of 3 to 6 that were sustained for over 2 hours in buffer pH 1.6, 5.0 and FeSSIF. The lowest σ_{max}values observed at pH 6.5 reached σ_{max} of 1.7 for MLX-SLC and 1.5 for MLX-MLE. Increasing drug solubility with increasing pH leads to lower supersaturation generation rates, lower σ_{max}, and lower de-supersaturation rates. Similar behavior has been observed with amorphous solid dispersions (Sun and Lee, 2013).

Figure 6

Examining the results in terms of Do and SA (Fig. 7) demonstrates that the dose was below cocrystal solubility (Do<SA) except at pH 1.6. This means that cocrystal solubility is adequate to dissolve the dose at all other pH values. Both Do and SA are normalized by drug solubility and their comparison can be interpreted in terms of dose

and cocrystal solubility. It is also shown that Do and SA influence σ_{max}, RAUC, and the shape of drug release curves. σ_{max} and RAUC decrease with decreasing Do as pH increases.

Figure 7

The very slow de-supersaturation rate of MLX-SLC at pH 1.6 and 5.0 appears to be due to the interplay between cocrystal dissolution and drug crystallization. This cocrystal has a Do>>SA at pH 1.6 and cocrystal dissolution is likely to be incomplete. This behavior is the subject of a manuscript in preparation. The superior in vivo absorption rate of MLX-SLC cocrystal compared to drug and to MLX-MLE in rats (Weyna et al., 2012), appears to be a result of this dissolution-crystallization quasi-equilibrium. A recent publication (Skrdla et al., 2020) modeled similar behavior following the dissolution of amorphous drugs.

At pH 6.5, Do<<SA and the cocrystal solubility is more than adequate to dissolve the dose. Furthermore, Do values (2.3 and 2.4) are the closest to σ_{max} (1.7 and 1.5) for SLC and MLE cocrystals at this pH and a large fraction of the cocrystal added was dissolved to reach σ_{max}. The ratio of σ_{max}/Do represents that the fraction of cocrystal dissolved is at least 0.7 for SLC and 0.6 for MLE. Since there may be drug precipitation around σ_{max} the fraction of cocrystal dissolved can be above this estimate. It is important to consider Do and SA when analyzing drug release during cocrystal dissolution as both parameters are likely to influence the observed behavior and in some cases limit σ_{max}.

3.6 Wettability of drug and cocrystals

Poor wettability of drug and cocrystals was observed during dissolution studies in buffer pH 1.6 and 5.0, while in FeSSIF, wetting was greatly improved. Contact angle measurements quantify this improvement as shown in Table 5. Contact angles in blank FeSSIF pH 5.0 vs FeSSIF pH 5.0 decreased from 98.1° to 30.6° for MLX, from 101.4° to 29.1° for MLX-SLC and from 56.1° to 26.3° for MLX-MLE. The contact angles for MLX-MLE were lower than for MLX-SLC, consistent with MLE hydrophilic nature and high cocrystal SA. Although MLX-SLC is more soluble than the drug, its contact angles were relatively high. According to the literature, SLC has poor wetting properties, and contact angles of 103 and 105° in water, which may influence cocrystal wettability (Kaeashima et al., 1982; Lerk et al., 1976). Poor wettability of drug has been reported in water, a limiting factor in its dissolution (Pomázi et al., 2011).

Table 5. Contact angles of drug and cocrystals.

Samples	Contact angle (degrees °)			
	Buffer pH 1.6	Blank FeSSIF pH 5.0	FeSSIF pH 5.0	Buffer pH 6.5
MLX	89.9 ± 1.4	98.1 ± 2.9	30.6 ± 1.6	89.8 ± 5.9
MLX-SLC	106.4 ± 0.7	101.4 ± 2.3	29.1 ± 2.4	92.6 ± 6.8
MLX-MLE	50.2 ± 5.6	56.1 ± 5.5	26.3 ± 3.5	54.5 ± 0.5

3.7 Drug crystallization pathways

Cocrystal dissolution, drug nucleation and growth were investigated by *in situ* inverted microscopy. Cocrystal to drug conversion was found to occur on the cocrystal surface and in the bulk solution. The surface mediated conversion occurred via an intermediate metastable polymorph of MLX (Form IV). This behavior was observed only in buffer media at all pH conditions. It did not occur in FeSSIF.

Figure 8 shows photomicrographs demonstrating the surface nucleation of MLX IV and the associated Raman spectra. MLX IV dissolves as the stable Form I nucleates

and grows in the bulk solution. Raman spectra for these polymorphs have been previously reported (Coppi L., Sanmarti B., 2005; Luger et al., 1996). Raman spectra of MLX-SLC, MLX-MLE e MLX stable form are included in the supplementary material (Figure S6).

Figure 8

Table 6 summarizes the crystallization pathways of MLX during cocrystal dissolution determined by microscopy. Photomicrographs are included in supplementary material (Figure S7). Results show that drug precipitation was earlier for the more soluble cocrystal, MLE, and surface nucleation shortened the onset of cocrystal to drug conversion for both cocrystals. The influence of surface nucleation on drug supersaturation during dissolution of metastable solids has been reported (Box et al., 2016; Greco and Bogner, 2011). Less extent of surface nucleation was observed for both cocrystals at pH 1.6, where SA values are lowest. Given that SA (interfacial and bulk) for both cocrystals is much greater than MLX σ_{max}, nucleation is favorable in both interfacial and bulk domains, although bulk is greater than interfacial SA.

Table 6. Drug crystallization pathways during cocrystal dissolution.

Cocrystal	Dissolution Media (bulk pH)	Nucleation[a]	MLX polymorph precipitation[b]	Onset of crystallization time[c] (min) stirring
MLX-SLC	Buffer pH 1.6	Surface bulk	IV I	20 45
	Blank FeSSIF pH 5.0	Surface bulk	IV I	5 10
	FeSSIF pH 5.0	bulk	I	25
	Buffer pH 6.5	Surface bulk	IV I	5 5
	Buffer pH 1.6	Surface bulk	IV I	5 10
	Blank FeSSIF	Surface	IV	1

MLX-MLE	pH 5.0	bulk	I	10
	FeSSIF pH 5.0	bulk	I	10
	Buffer pH 6.5	Surface	IV	1
		bulk	I	5

[a]Nucleation behavior was determined from microscopy studies.
[b] MLX metastable polymorph IV precipitates on the surface of the dissolving cocrystal and then converts to MLX polymorph I (stable form) which precipitates in the bulk in buffer pH 1.6, blank FeSSIF pH 5.0 and buffer pH 6.5. The total conversion of polymorph IV to I occurred after 4h. No polymorph IV precipitation was observed in FeSSIF
[c]Time in which the drug was observed to precipitate for the first time.

4. Conclusion

Cocrystals can be classified in terms of thermodynamic parameters that influence the overall kinetic processes which include cocrystal dissolution, drug supersaturation and precipitation. In this study, we evaluated cocrystal properties (K_{eu}, SA, and interfacial pH) and compared them with biopharmaceutical drug properties (dose and dose/solubility ratio (Do)) to understand how they influence drug release kinetics. The interfacial pH of dissolving cocrystals is shown to be modulated by the coformer acidity, with MLE exhibiting a lower interfacial pH (1.6) than SLC cocrystal (4.5), diminishing the dissolution dependence of pH compared to the drug. Results reveal that Do and SA are important parameters to consider when analyzing drug release during cocrystal dissolution. They explain the dissolution-precipitation interplay and the characteristics of the concentration/supersaturation vs time curves.

Credit author statement

Tatiane Cogo Machado: Conceptualization, Methodology, Investigation, Writing-Original draft preparation, Reviewing and Editing.

Gislaine Kuminek: Methodology, Visualization, Writing-Reviewing and Editing.

Simone Gonçalves Cardoso: Funding acquisition, Supervision, Resources, Writing-Reviewing and Editing.

Nair Rodriguez-Hornedo: Conceptualization, Methodology, Supervision, Resources, Writing-Original draft preparation, Review and Editing.

Acknowledgments

The authors gratefully acknowledge the Brazilian governmental agencies Coordenação de Aperfeiçoamento de Pessoal de Nível Superior (CAPES) and Conselho Nacional de Desenvolvimento Científico e Tecnológico (CNPq) for the financial support, and Taynara Scherer and the Department of Food Engineering (Universidade Federal de Santa Catarina) for the contact angles analysis.

References

Alhalaweh, A., Ali, H.R.H., Velaga, S.P., 2014. Effects of polymer and surfactant on the dissolution and transformation profiles of cocrystals in aqueous media. Cryst. Growth Des. 14, 643–648. https://doi.org/10.1021/cg4015256

Amidon, G.L., Lennernas, H., Shah, V.P., Crison, J.R., 1995. A Theoretical Basis for a Biopharmaceutic Drug Classification: The Correlation of in Vitro Drug Product Dissolution and in Vivo Bioavailability. Pharm. Res. An Off. J. Am. Assoc. Pharm. Sci. 12, 413–419. https://doi.org/10.1023/A:1016212804288

Badran, M.M., Taha, E.I., Tayel, M.M., Al-Suwayeh, S.A., 2014. Ultra-fine self nanoemulsifying drug delivery system for transdermal delivery of meloxicam: Dependency on the type of surfactants. J. Mol. Liq. 190, 16–22. https://doi.org/10.1016/j.molliq.2013.10.015

Berry, D.J., Steed, J.W., 2017. Pharmaceutical cocrystals, salts and multicomponent systems; intermolecular interactions and property based design. Adv. Drug Deliv. Rev. 117, 3–24. https://doi.org/10.1192/bjp.111.479.1009-a

Bevernage, J., Brouwers, J., Brewster, M.E., Augustijns, P., 2013. Evaluation of gastrointestinal drug supersaturation and precipitation: Strategies and issues. Int. J. Pharm. 453, 25–35. https://doi.org/10.1016/j.ijpharm.2012.11.026

Box, K.J., Comer, J., Taylor, R., Karki, S., Ruiz, R., Price, R., Fotaki, N., 2016. Small-Scale Assays for Studying Dissolution of Pharmaceutical Cocrystals for Oral Administration. AAPS PharmSciTech 17, 245–251. https://doi.org/10.1208/s12249-015-0362-5

Cao, F., Amidon, G.L.., Rodriguez-Hornedo, N., Amidon, G.E., 2016. Mechanistic Analysis of Cocrystal Dissolution as a Function of pH and Micellar Solubilization. Mol. Pharm. 13, 1030–1046. https://doi.org/10.1021/acs.molpharmaceut.5b00862

Cao, F., Rodriguez-Hornedo, N., Amidon, G.E., 2019. Mechanistic Analysis of Cocrystal Dissolution, Surface pH, and Dissolution Advantage as a Guide for Rational Selection. J. Pharm. Sci. 108, 243–251. https://doi.org/10.1192/bjp.112.483.211-a

Cavanagh, K.L., Maheshwari, C., Rodríguez-Hornedo, N., 2018. Understanding the Differences Between Cocrystal and Salt Aqueous Solubilities. J. Pharm. Sci. 107, 113–120. https://doi.org/10.1016/j.xphs.2017.10.033

Chen, Y., Rodríguez-Hornedo, N., 2018. Cocrystals Mitigate Negative Effects of High pH on Solubility and Dissolution of a Basic Drug. Cryst. Growth Des. 18, 1358–1366. https://doi.org/10.1021/acs.cgd.7b01206

Cheney, M.L., Weyna, D.R., Shan, N., Hanna, M., Wojtas, L., Zaworotko, M.J., 2010. Supramolecular Architectures of Meloxicam Carboxylic Acid Cocrystals, a Crystal Engineering Case Study. Cryst. Growth Des. 4401–4413. https://doi.org/10.1021/cg100514g

Coppi L., Sanmarti B., C.M., 2005. United States Patent No .: US 6,967,248 B2. Crystalline forms of meloxicam and processes for their preparation and interconversion. 2, 1–14.

Davies, N.M., Anderson, K.E., 1997. Clinical pharmacokinetics of naproxen. Clin. Pharmacokinet. 32, 268–293. https://doi.org/10.2165/00003088-199732040-00002

Dawson, R.M.C., Elliott, D.C., Elliott, W.H., Jones, K.M., 1960. Data for biochemical research 8, A490. https://doi.org/https://doi.org/10.1021/ed037pA490.3

Del Tacca, M., Colucci, R., Fornai, M., Blandizzi, C., 2002. Efficacy and Tolerability of

Meloxicam , a COX-2 Preferential Nonsteroidal Anti-Inflammatory Drug A Review. Clin. Drug Invest 22, 799–818. https://doi.org/DOI: 10.2165/00044011-200222120-00001

Ghorab, M.M., Abdel-salam, H.M., El-sayad, M.A., Mekhel, M.M., 2004. Tablet Formulation Containing Meloxicam and β -Cyclodextrin : Mechanical Characterization and Bioavailability Evaluation 5, 1–6.

Good, D.J., Rodríguez-Hornedo, N., 2009. Solubility advantage of pharmaceutical cocrystals. Cryst. Growth Des. 9, 2253–2264. https://doi.org/10.1021/cg801039j

Greco, K., Bogner, R., 2011. Solution-Mediated Phase Transformation: Significance During Dissolution and Implications for Bioavailability. J. Pharm. Sci. 1–23. https://doi.org/DOI: https://doi.org/10.1002/jps.23025

Huang, Y., Kuminek, G., Roy, L., Cavanagh, K., Yin, Q., Rodriguez-Hornedo, N., 2019. Cocrystal Solubility Advantage Diagrams as a Means to Control Dissolution, Supersaturation, and Precipitation. Mol. Pharm. 16, 3887–3895. https://doi.org/10.1021/acs.molpharmaceut.9b00501

Kaeashima, Y., Okumura, M., Takaneka, H., 1982. Spherical Crystallization : Direct Spherical Agglomeration of Salicylic Acid Crystals During Crystallization Calcium Carbonate Hexahydrate from Organic-Rich Sediments of the Antarctic Shelf : Precursors of Glendonites. Science (80-.). 216, 1–2.

Kuminek, G., Cao, F., Rocha, A.B.O., Cardoso, S.G., Rodriguez-Hornedo, N., 2016. Cocrystals to facilitate delivery of poorly soluble compounds beyond-rule-of-5. Adv. Drug Deliv. Rev. 101, 143–166. https://doi.org/10.1016/j.addr.2016.04.022

Kuminek, G., Rodríguez-Hornedo, N., Siedler, S., Rocha, H.V.A., Cuffini, S.L., Cardoso, S.G., 2016. How cocrystals of weakly basic drugs and acidic coformers might modulate solubility and stability. Chem. Commun. 52, 5832–5835. https://doi.org/10.1039/c6cc00898d

Lakshman, D., Chegireddy, M., Hanegave, G., NayyaSree, K., Kumar, N., Lewis, S., Dengale, S., 2020. Investigation of drug-polymer miscibility, biorelevant dissolution, and bioavailability improvement of Dolutegravir-polyvinyl caprolactam-polyvinyl acetate-polyethylene glycol graft copolymer solid dispersions. Eur. J. Pharm. Sci. 142, 105–137. https://doi.org/https://doi-org.proxy.lib.umich.edu/10.1016/j.ejps.2019.105137

Lerk, C.F., Schoonen, A.J.M., Fell, J.T., 1976. Contact Angles and Wetting of Pharmaceutical Powders. J. Pharm. Sci. 65, 843–847.

Leyssens, T., Horst, J.H., 2018. Solution co-crystallisation and its applications, in: Tiekink, E., Zukerman-Schpector, J. (Eds.), Multi-Component Crystals. Walter de Gruyter GmbH, Berlin/Boston Coverf, Berlin/Boston, pp. 205–236. https://doi.org/10.1002/9781119109785.pubnote

Lipert, M.P., Rodríguez-Hornedo, N., 2015. Cocrystal transition points: Role of cocrystal solubility, drug solubility, and solubilizing agents. Mol. Pharm. 12, 3535−3546. https://doi.org/10.1021/acs.molpharmaceut.5b00111

Lipert, M.P., Roy, L., Childs, S.L., Rodríguez-Hornedo, N., 2015. Cocrystal Solubilization in Biorelevant Media and its Prediction from Drug Solubilization. J. Pharm. Sci. 104, 4153–4163. https://doi.org/10.1002/jps.24640

Luger, P., Daneck, K., Engel, W., Trummlitz, G., Wagner, K., 1996. Structure and physicochemical properties of meloxicam, a new NSAID. Eur. J. Pharm. Sci. 4,

175–187. https://doi.org/10.1016/0928-0987(95)00046-1
Machado, T.C., Gelain, A.B., Rosa, J., Cardoso, S.G., Caon, T., 2018. Cocrystallization as a novel approach to enhance the transdermal administration of meloxicam. Eur. J. Pharm. Sci. 123, 184–190. https://doi.org/10.1016/j.ejps.2018.07.038
Mooney, K.G., Mintun, M.A., Himmelstein, K.J., Stella, V.J., 1981. Dissolution kinetics of carboxylic acids I: Effect of pH under unbuffered conditions. J. Pharm. Sci. 70, 13–22. https://doi.org/10.1002/jps.2600700103
Ochi, M., Inoue, R., Yamauchi, Y., Yamada, S., Onoue, S., 2013. Development of meloxicam salts with improved dissolution and pharmacokinetic behaviors in rats with impaired gastric motility. Pharm. Res. 30, 377–386. https://doi.org/10.1007/s11095-012-0878-2
Ochi, M., Kawachi, T., Toita, E., Hashimoto, I., Yuminoki, K., 2014. Development of nanocrystal formulation of meloxicam with improved dissolution and pharmacokinetic behaviors 474, 151–156. https://doi.org/doi: 10.1016/j.ijpharm.2014.08.022
Oh, D., Curl, R.L., Amidon, G.L., 1993. Estimating the fraction dose absorbed from suspensions of poorly soluble compounds in humans: A mathematical model. Pharm. Res. 10, 264–270.
Pomázi, A., Ambrus, R., Sipos, P., Szabó-Révész, P., 2011. Analysis of co-spray-dried meloxicam-mannitol systems containing crystalline microcomposites. J. Pharm. Biomed. Anal. 56, 183–190. https://doi.org/10.1016/j.jpba.2011.05.008
Rinaki, E., Dokoumetzidis, A., Valsami, G., Macheras, P., 2004. Identification of Biowaivers Among Class II Drugs: Theoretical Justification and Practical Examples. Pharm. Res. 21, 1567–72. https://doi.org/DOI: 10.1023/B:PHAM.0000041450.25106.c8
Rodríguez-Hornedo, N., Nehm, S.J., Seefeldt, K.F., Pagán- Torres, Y., Falkiewicz, C.J., 2006. Reaction crystallization of pharmaceutical molecular complexes. Mol. Pharm. 3, 362–367. https://doi.org/10.1021/mp050099m
Rosa, J., Machado, T.C., da Silva, A.K., Kuminek, G., Bortolluzzi, A.J., Caon, T., Cardoso, S.G., 2019. Isoniazid-Resveratrol Cocrystal: A Novel Alternative for Topical Treatment of Cutaneous Tuberculosis. Cryst. Growth Des. acs.cgd.9b00313. https://doi.org/10.1021/acs.cgd.9b00313
Schver, G.C.R.M., Lee, P.I., 2018. Combined Effects of Supersaturation Rates and Doses on the Kinetic-Solubility Profiles of Amorphous Solid Dispersions Based on Water-Insoluble Poly(2-hydroxyethyl methacrylate) Hydrogels. Mol. Pharm. 15, 2017–2026. https://doi.org/10.1021/acs.molpharmaceut.8b00162
Serajuddin, A.T.M., 2007. Salt formation to improve drug solubility. Adv. Drug Deliv. Rev. https://doi.org/10.1016/j.addr.2007.05.010
Skrdla, P.J., Floyd, P.D., Dell'Orco, P.C., 2020. Modeling Recrystallization Kinetics following the Dissolution of Amorphous Drugs. Mol. Pharm. 17, 219–228. https://doi.org/10.1021/acs.molpharmaceut.9b00940
Smith, A., 2001. The Merck index: an encyclopedia of chemicals, drugs, and biologicals. Merck, Whitehouse Stn. 2195–2198.
Sugano, K., Terada, K., 2015. Rate- and Extent-Limiting Factors of Oral Drug Absorption: Theory and Applications. J. Pharm. Sci. 104, 2777–2788. https://doi.org/10.1002/jps.24391

Sun, D.D., Lee, P.I., 2015. Haste Makes Waste: The Interplay Between Dissolution and Precipitation of Supersaturating Formulations. AAPS J. 17, 1317–1326. https://doi.org/10.1208/s12248-015-9825-6

Sun, D.D., Lee, P.I., 2013. Evolution of supersaturation of amorphous pharmaceuticals: The effect of rate of supersaturation generation. Mol. Pharm. 10, 4330–4346. https://doi.org/10.1021/mp400439q

Tanaka, Y., Sugihara, M., Kawakami, A., Imai, S., Itou, T., Murase, H., Saiki, K., Kasaoka, S., Yoshikawa, H., 2017. In vivo analysis of supersaturation/precipitation/absorption behavior after oral administration of pioglitazone hydrochloride salt; determinant site of oral absorption. Eur. J. Pharm. Sci. 106, 431–438. https://doi.org/10.1016/j.ejps.2017.06.011

Taylor, L.S., Zhang, G.G.Z., 2016. Physical chemistry of supersaturated solutions and implications for oral absorption |. Adv. Drug Deliv. Rev. 101, 122–142.

Türck, D., Busch, U., Heinzel, G., Narjes, H., Nehmiz, G., 1995. Effect of Food on the Pharmacokinetics of Meloxicam after Oral Administration. Clin. Drug Investig. 9, 270–276. https://doi.org/10.2165/00044011-199509050-00004

Ullah, I., Baloch, M.K., Durrani, G.F., 2011. Solubility of nonsteroidal anti-inflammatory drugs (NSAIDs) in aqueous solutions of non-ionic surfactants. J. Solut. Chem. 40, 1341–1348. https://doi.org/10.1007/s10953-011-9709-z

Weyna, D.R., Cheney, M.L., Shan, N., Hanna, M., Zaworotko, M.J., Sava, V., Song, S., Sanchez-Ramos, J.R., 2012. Improving solubility and pharmacokinetics of meloxicam via multiple-component crystal formation. Mol. Pharm. 9, 2094–2102. https://doi.org/10.1021/mp300169c

Figure captions

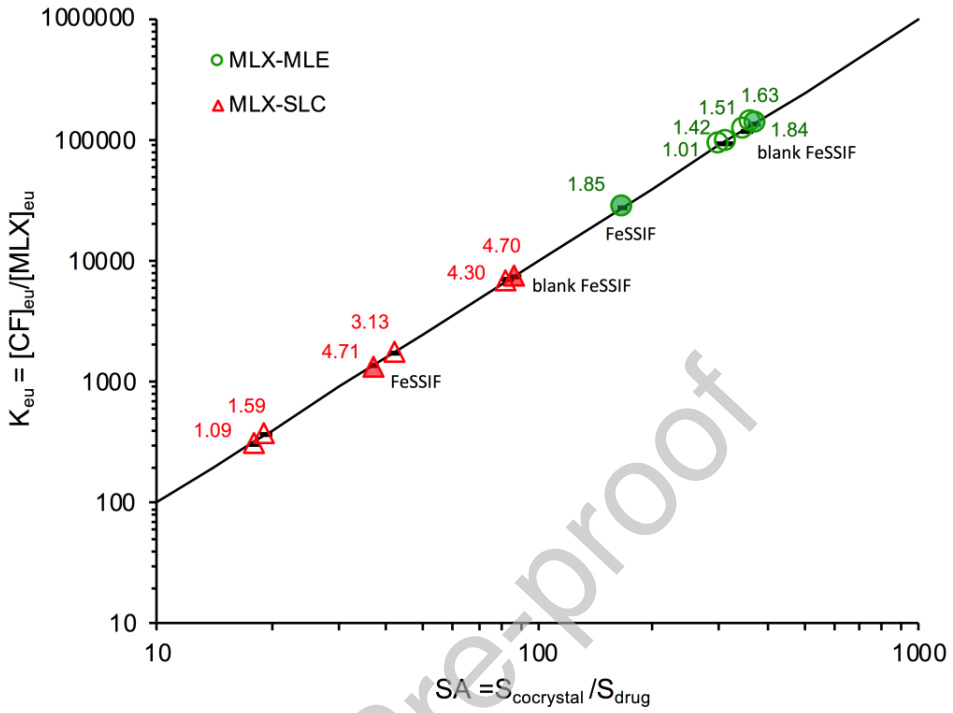

Figure 1. Relationship between K_{eu} and SA for MLX cocrystals. The line was generated according to the log form of Eq. (6). Numbers next to data points indicate equilibrium or eutectic pH values. Symbols represent experimentally determined K_{eu} and SA values of MLX-MLE (green circles) and MLX-SLC (red triangles). Filled symbols represent blank FeSSIF and FeSSIF as indicated in plot. Standard errors are within the experimental points and are less than 5%. K_{eu} and SA increase in blank FeSSIF with increasing pH due to coformer ionization and decrease in FeSSIF due to drug solubilization. MLE cocrystal has higher K_{eu} and SA than SLC cocrystal.

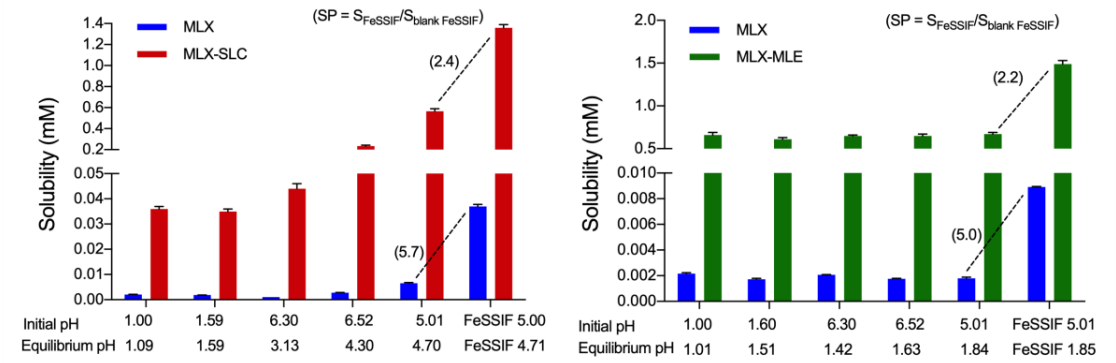

Figure 2. Drug and cocrystal solubilities increase with equilibrium pH and the presence of FeSSIF. Cocrystal solubilities were determined from eutectic point measurements according to Eq. (1). Cocrystal solubilities are higher than S_{drug} in all conditions studied. Solubilization by FeSSIF is consistent with the square-root relationship $SP_{cocrystal} = \sqrt{SP_{drug}}$. Numbers in parenthesis represent the solubilization power ($SP = S_{FeSSIF}/S_{blank.\ FeSSIF}$). S_{FeSSIF} is the sum of the concentration of all species dissolved (aqueous and micellar) from cocrystals or drug solubility experiment in FeSSIF. $S_{blank\ FeSSIF}$ is the drug or cocrystal solubility at initial pH 5.0 buffer in the absence of solubilizing agents.

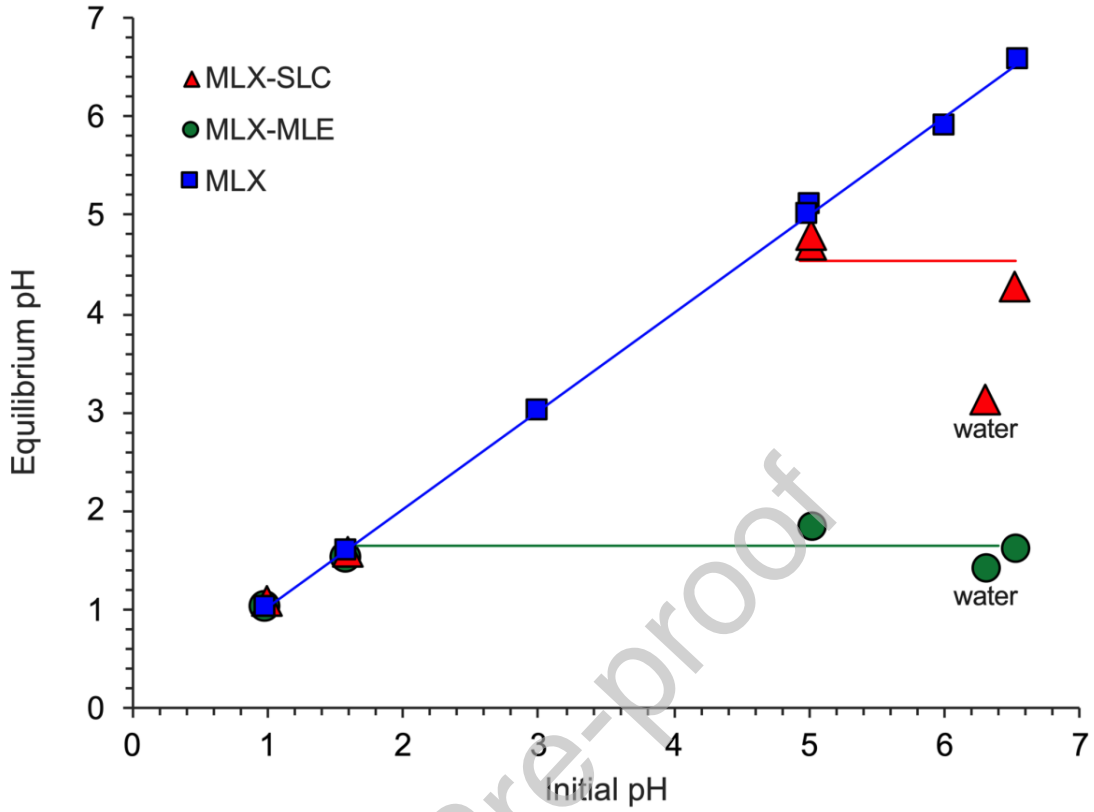

Figure 3. Initial and equilibrium pH values from drug solubility and eutectic point measurements of cocrystal solubility. Initial pH represents bulk pH and equilibrium pH represents microenvironment pH. Cocrystals lowered the microenvironment pH compared to bulk as a result of the component ionization properties. Microenvironment pH was modulated to around 1.6 by MLE cocrystal and to around 4.5 by SLC cocrystal at bulk pH values at or above the microenvironment pH values.

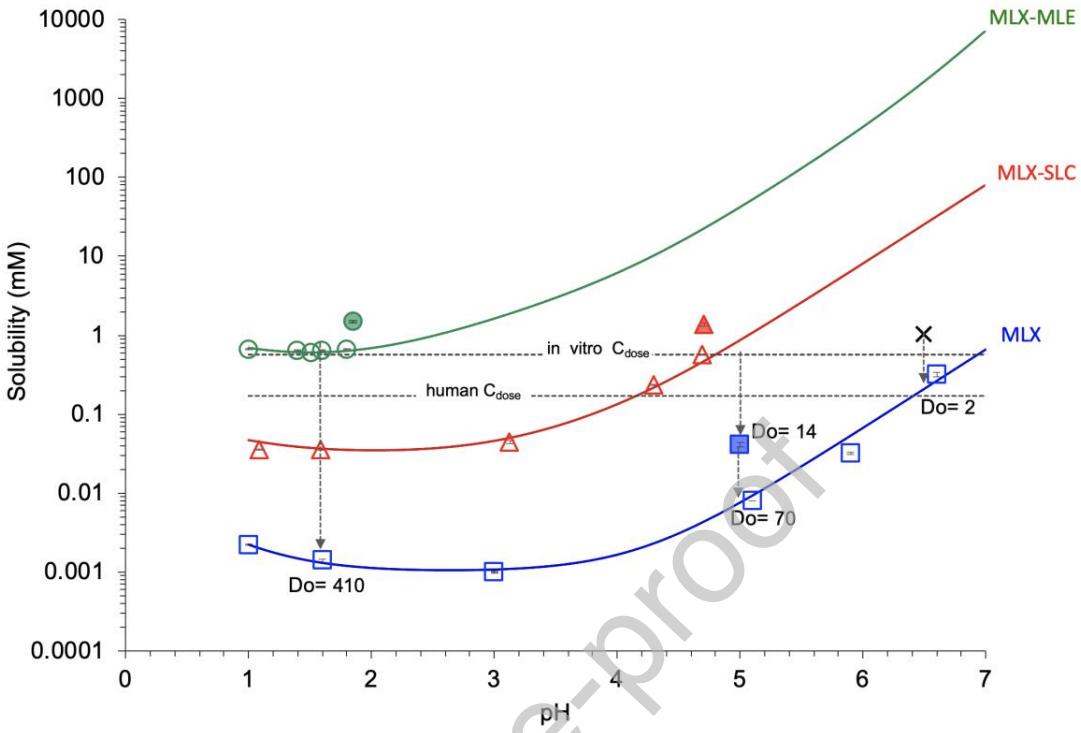

Figure. 4 Solubility-pH dependence of drug and cocrystals. Symbols represent experimentally determined solubilities from equilibrium measurements. Filled symbols represent drug and cocrystals solubility in FeSSIF. Cocrystal solubility curves were generated using Eqs. (7), (8) and (9). pH values correspond to equilibrium pH. Dose concentrations (C_{dose}) corresponding to human dose (0.17 mM), and in vitro concentration (0.57 mM) in the present dissolution study. X represents the in vitro C_{dose} in dissolution studies from another lab (Weyna et al., 2012). Drug dose/solubility ratios, Do, in buffer pH 1.6, 5.0, 6.5 and FeSSIF pH 5.0 are indicated by the arrows and were calculated using Eq. (5).

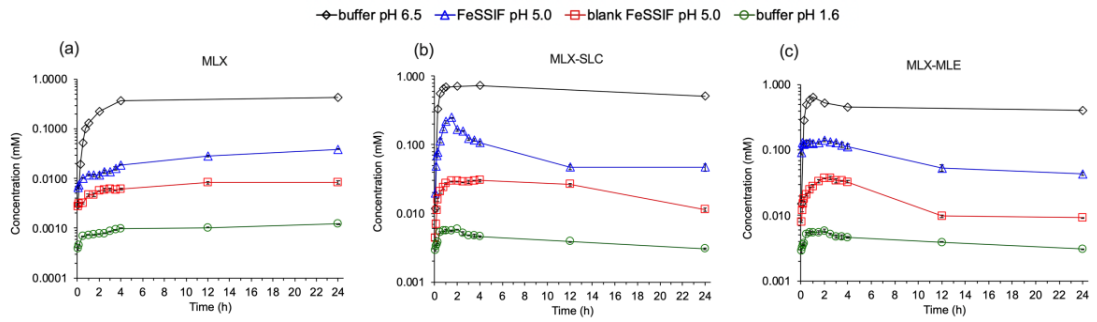

Figure 5. Dissolution profiles for (a) MLX (b) MLX-SLC and (c) MLX-MLE in buffer pH 1.6, 5.0, 6.5 and FeSSIF pH 5.0. Cocrystals achieved drug concentrations much higher than those achieved by drug dissolution. The changes between the initial and final dissolution pH were not statistically significant ($p>0.05$). Concentrations in buffer pH 6.5 are from Weyna et al., (Weyna et al., 2012). Final dissolution pH with initial pH 6.5 was not reported.

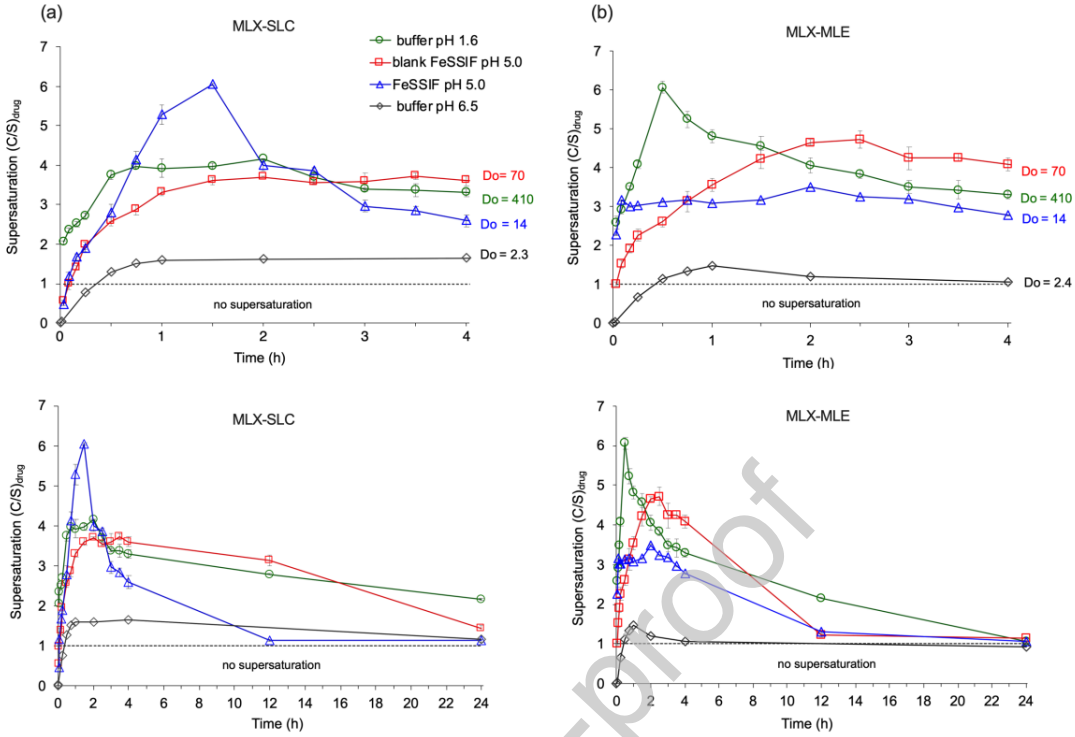

Figure. 6 Supersaturation profiles for (a) MLX-SLC and (b) MLX-MLE in buffer pH 1.6, 5.0, 6.5, and FeSSIF pH 5.0 the first 4h (top) and 24 h (bottom). Do values for all dissolution conditions are indicated. Supersaturation levels in buffer pH 6.5 were calculated from Weyna et al. (Weyna et al., 2012).

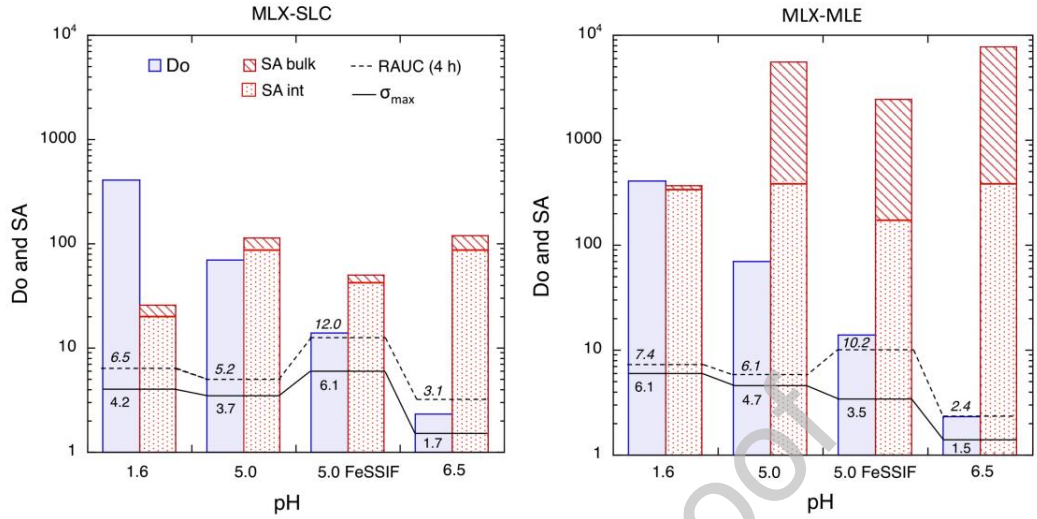

Figure 7. Dose solubility ratio ($Do=C_{dose}/S_{drug}$) and cocrystal solubility advantage ($SA=S_{cocrystal}/S_{drug}$) for SLC and MLE cocrystals in the dissolution media studied. SA is higher for MLE and its interfacial SA is reduced significantly to a constant value. Do and SA influence the shape of drug release curves, σ_{max} and RAUC.

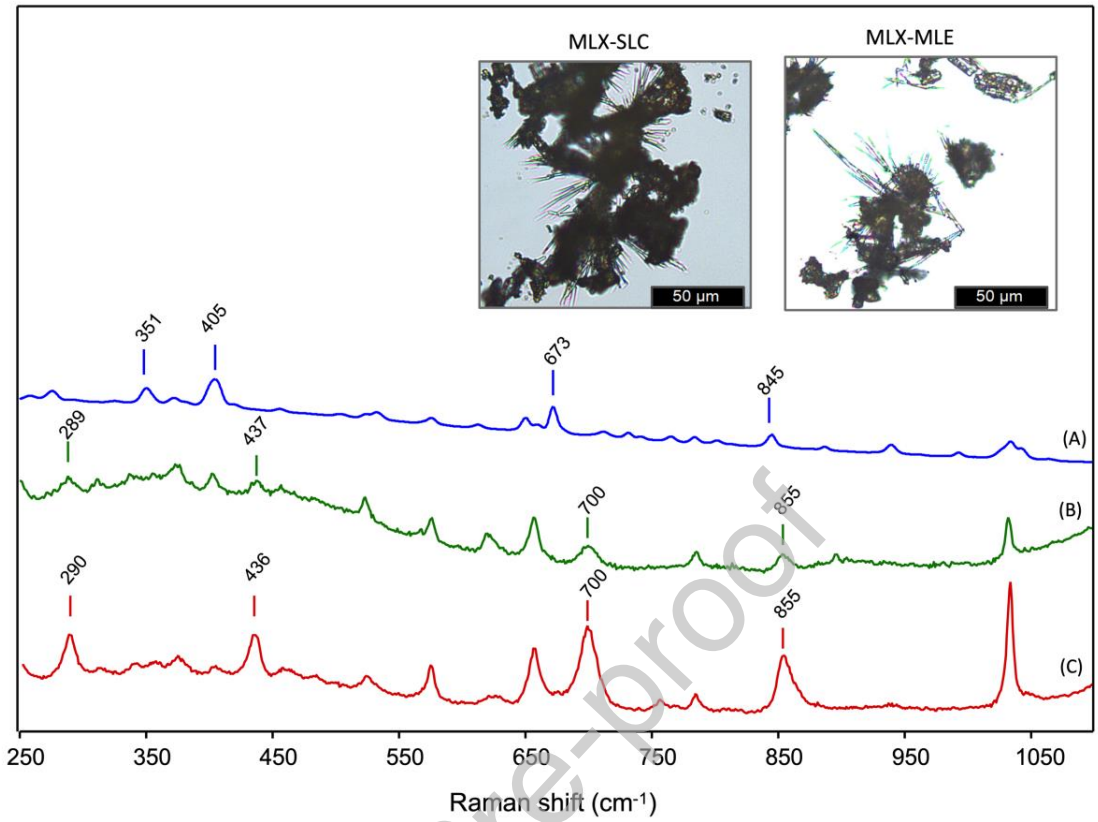

Figure 8. Raman spectra of the drug phases precipitated in the bulk solution (A) and on the surface of the dissolving cocrystals MLX-MLE (B) and MLX-SLC (C). Spectra indicate that bulk solution precipitation is MLX polymorph I, and needle-like crystals formed on the surface of dissolving cocrystals as shown in photomicrographs are MLX polymorph IV.

Graphical Abstract